Dynamic Properties of Boron Carbide

by

Jiajie Huang

A thesis submitted to Johns Hopkins University in conformity with the

requirements for the degree of Master of Science

Baltimore, Maryland

May, 2019

Abstract

Boron carbide (BC) is potentially useful as a lightweight armor material, but its penetration resistance drops under dynamic impact, the reasons for which are not entirely understood. To examine the mechanisms of failure under dynamic loading, we subjected samples of boron carbide to uniaxial compression at strain rates of up to 10^4 s^{-1} while visualizing the failure in real time using x-ray phase contrast imaging (XPCI) at the Advanced Photon Source. However, we can only record 2D images during dynamic loading, as the crack density increases it becomes difficult to track individual defects and understand the failure processes. Since the intensity variations in XPCI encode information about the 3D crack size distribution (CSD), a physics-based model is used to try to extract this information, which is potentially useful to show how it correlates with dynamic crack propagations and distributions from XPCI.

Primary Reader: Todd C. Hufnagel

Acknowledgements

This work was supported by the Army Research Laboratory under Cooperative Agreement No. W911NF-12-2-0022. The content, views, and conclusions contained in this document are those of the author and should not be interpreted as representing the official positions or policies, either expressed or implied, of the Army Research Laboratory, or the U.S. Government. The U.S. Government is authorized to reproduce and distribute reprints for government purposes notwithstanding any copyright notation herein. This research used resources of the Advanced Photon Source, a DOE Office of Science User Facility operated for the DOE Office of Science by Argonne National Laboratory under contract no. DE-AC02-06CH11357.

The following people had a significant influence on this thesis: Andrew F.T. Leong and Todd C. Hufnagel.

I'd also like to thank: Jason Parker, Amartya Bhattacharjee, Hao Sheng, Ming Guan, Qinglei Zeng, Nick Sinclair, Xianghui Xiao, Brian E. Schuster, and Daniel T. Casem.

Content

List of Tables

List of figures

1. Introduction

Boron carbide is a promising ceramic material with superior hardness, low density, and good chemical stability [1-4]. It has already attracted tremendous attention due to the potential application of body armor, abrasives, nuclear shielding, and thermal refractory.

The microstructure and the static mechanical properties of boron carbide has been studied over decades to understand the mechanism behind its special properties [1-4,6,7]. There was a wide debate on the stoichiometry of boron carbide [22-25]. A recent study showed that boron carbide is composed of 12-atom icosahedra linked by 3-atom chain [22]. For B_4C, the icosahedra usually consists of 11 boron atoms and 1 carbon atom, and the chain consists of 2 carbon atoms on the side and 1 boron atom in the middle due to the lowest free energy of this structure. On the other hand, extensive efforts have been devoted to static mechanical properties such as compressive strength, flexural strength, hardness, and fracture toughness. [1-14, 18-23]

Dynamic properties however, which are closer to application of body armor, have not been widely studied. More importantly, the penetration resistance of boron carbide drops under dynamic impact, the reasons for which are not entirely understood [26].

In this work, we cut 2mm×2mm×2mm cubic boron carbide samples by high speed saw and diamond wire, and polished them by polishing paper(finished by 1mm). At the Advanced Photon Source(APS), dynamic properties of boron carbide were measured by Kolsky bar uniaxial

compressive test at strain rates of up to 10^4 s^{-1}, and the fracture behavior is visualized with x-ray phase contrast imaging technique. The damage extent of the material is analyzed using a physics-based model proposed by A. F. T. Leong [15].

However, we can only record 2D images during dynamic loading, as the crack density increases it becomes difficult to track individual defects and understand the failure processes. Since the intensity variations in XPCI encode information about the 3D crack size distribution (CSD), a physics-based model is used to try to extract this information, which is potentially useful to show how it correlates with dynamic crack propagations and distributions from XPCI.

2. Background

2.1 Mechanical properties of boron carbide

At room temperature, boron carbide has a density of 2.30-2.55g/cm^3, Vickers hardness of 38-44 GPa, flexural strength of 320-450 MPa, fracture toughness of 3.0-4.0 MPa·$m^{1/2}$, compressive strength of 2.8-5.4 GPa and Young's Modulus of 3.6-4.7 GPa [7,18-23]. Excellent hardness and low density of boron carbide have attracted extensive researchers in the past 20 years. [1-14, 18-23]

Swab, JJ [6] etc. found no significant difference of compression strength under between static and low strain rate loading. But the compression strength under high strain rate is much higher than under low strain rate. [5,7] Hayun [7] etc. showed that SPS-processed boron carbide, which is closer to theoretical density, displays higher static and dynamic mechanical properties. The reason is because of the lower porosity and the smaller grain size of SPS-processed boron carbide compared with boron carbide processed in other method.

2.2 Kolsky bar uniaxial compression test technique

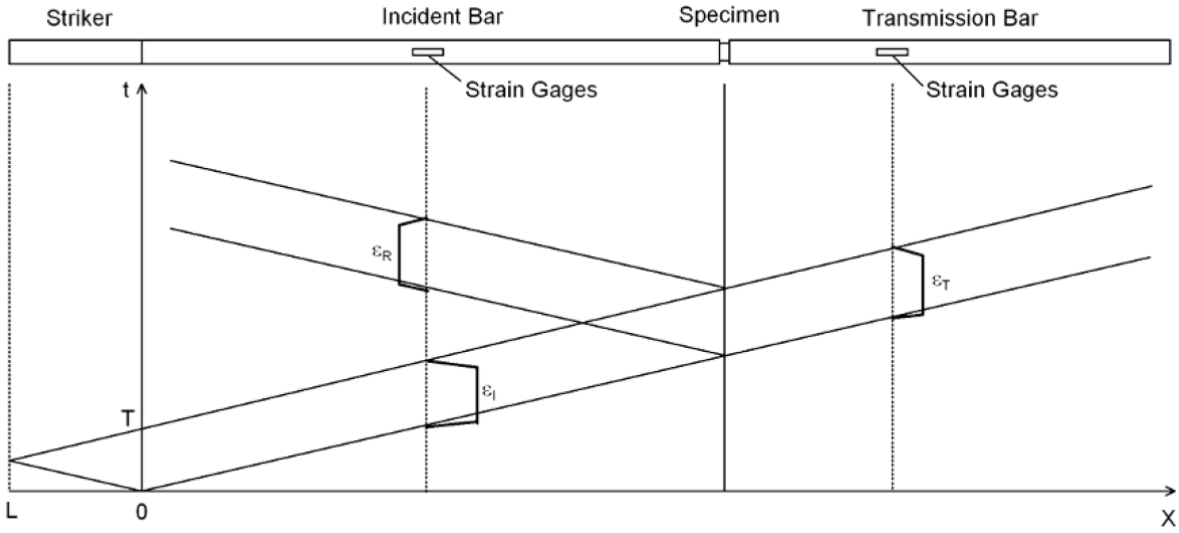

Fig.1 X-t diagram of stress wave propagation in a Kolsky bar system [16]

The Kolsky compression bar system is shown in Fig.1. A compression wave generated by the striker is transmitted in the incident bar, recorded by the strain gages on incident bar before reaching the free end of incident bar. Then part of the compression wave is reflected at the free end as a tension wave, recorded by strain gages on incident bar again, and the rest of wave is transmitted back to the transmission bar, recorded by the strain gages on transmission bar. Since the original compression wave typically last for a few microseconds, all the signals recorded on strain gages last for a few microseconds. The loading duration, T , produced in a Kolsky bar experiment is determined by the striker length, L.

$$T = \frac{2L}{C_{st}}$$

where C_{st} is the elastic wave speed of the striker material.

We can calculate the average strain rate of specimen by

$$\dot{\varepsilon} = \frac{C_B}{L_s}(\varepsilon_I - \varepsilon_R - \varepsilon_T)$$

where L_s is the length of specimen, and C_B is the elastic bar wave speed of the bar material. Thus the strain can be calculated from

$$\varepsilon = \int_0^t \dot{\varepsilon} dt = \frac{C_B}{L_S} \int_0^t (\varepsilon_I - \varepsilon_R - \varepsilon_T) dt$$

To calculate the stress, there are two methods based on either incident bar or transmission bar. Based on signal on incident bar, the stress can be calculated from

$$\sigma_1 = \frac{A_B}{A_S} E_B (\varepsilon_I + \varepsilon_R)$$

Based on signal on transmission bar, the stress can be calculated from

$$\sigma_2 = \frac{A_B}{A_S} E_B \varepsilon_T$$

where A_B is the cross-sectional areas of the bars, A_s is the cross-sectional areas of specimen, and E_B is Young's modulus of the bar material. Ideally, when the specimen deforms uniformly, stresses calculated from two strain gages would be the same. And we can also tell if the specimen deforms uniformly by comparing σ_1 and σ_2. If they are not the same, normally we take the average of σ_1 and σ_2 as the compressive stress of the specimen,

$$\sigma = (\sigma_1 + \sigma_2)/2$$

2.3 Physics-based model for 3D crack characterization

In the previous XPCI experiment, Feng [11] and Huang [12] conducted XPCI experiment to reveal the dynamic damage and fracture modes of glass and single crystal Si under high strain rates(10^2 -10^4 s^{-1}). Leong [13] utilized high contrast images from XPCI experiment to quantitively analyze lung air volumes inside human body to detect lung diseases based on a near-field x-ray diffraction

models he developed. Margie [27] visualized crack tip propagation in glass, laser-induced shock waves in water and electric arc ignition by X-ray phase-contrast imaging using synchrotron radiation for the first time. The visualizations could help to build stochastic crack propagation model, understand laser-induced liquid-jetting, and design specific electric fuses. Here, we use Leong's theory to model the specimen.

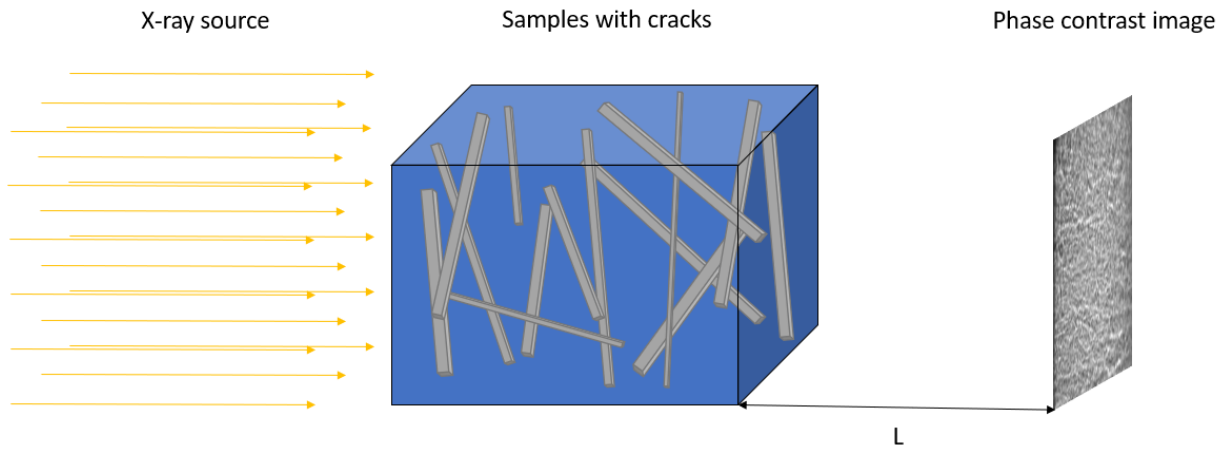

Fig.2. Model of boron carbide samples with cracks. The cracks are modeled as long cuboid voids, causing a phase shift of the X-ray beam, which is detected by an X-ray detector.

The cracks inside the sample are modeled as long cuboid voids (in grey). In the near-field diffraction regime, they meet following condition:

$$\left|F\left\{\frac{I(x,y,z=L)}{I(x,y,z=0)}-1\right\}\right|^2=\sum(L^2\delta^2{k_\perp}^4|8abc\mathrm{sinc}(a)\mathrm{sinc}(b)\mathrm{sinc}(c)|^2), \qquad (1)$$

where $\mathrm{I(x,y,z=0)}$ is the amplitude of absorption contrast image, $\mathrm{I(x,y,z=L)}$ is the amplitude of image captured by camera, F is the Fourier transform, L is the distance between sample and camera, δ is the refractive index decrement of boron carbide, $k_\perp=\sqrt{{k_x}^2+{k_y}^2}$ is the transverse wavenumber in the (x, y) plane for each crack (which means different orientation

of crack has different $k_{\perp}$), N is the number of cracks, and a, b, c are half of side length of cuboid cracks.

In order to recover the $\mathrm{I}(\mathrm{x},\mathrm{y},\mathrm{z}=0)$, we can use equation[17]:

$$\mathrm{I}(\mathrm{x},\mathrm{y},\mathrm{z}=0) = F^{-1}\left\{\frac{F[I(x,y,z=L)]}{1+\frac{\delta L}{\mu}k_{\perp}^{2}}\right\}$$

where F^{-1} is the inverse Fourier transform with respect to x and y, and μ is linear attenuation coefficient of boron carbide.

The left side of the equation (1) is calculated from the experimental result and the right side is the analytical result. Since we can calculate the experimental result, what we do next is to arbitrarily choose the distribution, orientation and number of cracks to calculate the right side to make it equal to experimental result. Thus, using this equation, we need to try different distribution, orientation and number of cracks to find out the result of crack distribution, orientation and number.

The parameters used to simulate phase contrast images are shown in Table 1.

Table 1. Parameters used for simulating phase contrast images

Pixel size	3.25 μm
Distance from sample to camera, L	0.73m
linear attenuation coefficient, μ	80.0m^{-1}
Refractive index decrement, δ	1.18e-06
Energy of X-ray source	20.4keV

3. Experimental Methods

3.1 Sample preparation

Commercial grade boron carbide was cut into slices by high speed saw (Allied High Tech Products, Inc.), and then cut into 1.5 mm cuboids by diamond wire saw (Agar Scientific Ltd.). Since boron carbide is very hard, it is easy for the diamond wire to go blunt, so it is recommended to change diamond wire frequently to keep high cutting efficiency.

In order to make sure the angle between adjacent sides are 90°, a small platform was used to achieve that, shown in Fig.3. The side of samples are stick to the protrude part of platform to make sure that the angle of adjacent sides close enough to 90°. Another benefit of using this of platform is that a dozen samples can be polished at the same time since the platform have enough space for more samples.

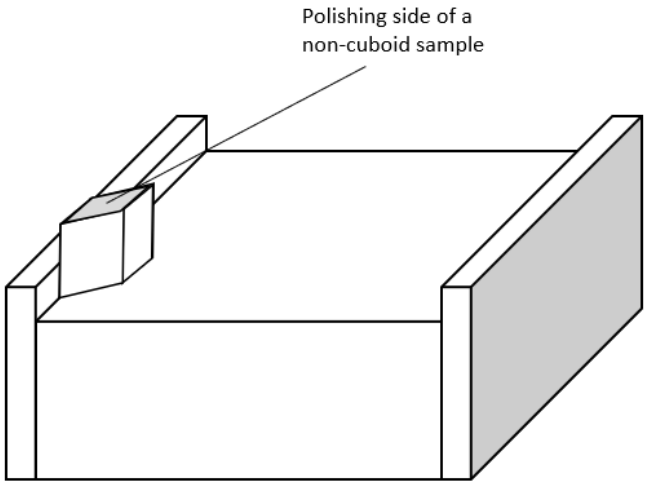

Fig.3. Cuboid preparation platform

When the sample was polished by polishing machine, we used 30, 15, 9, 6, 3 and 1 μm diamond lapping films successively (Allied High Tech Products, Inc.). During polishing, each step should last for at least 3 minutes to make sure there are no scratches on the sample. We polished all six faces to remove scratches that would cause stress concentration and significantly reduce the maximum stress during the experiment. The angle between adjacent sides should be in the range of 89°-91°, and the opposite sides should be perfectly parallel. The microscopic images of samples should look like Fig.4.

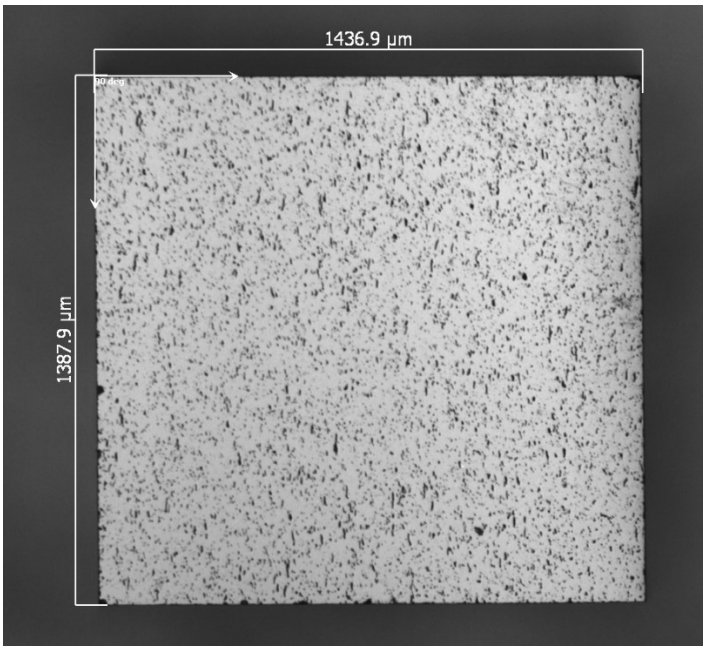

Fig.4. Microscopic image of finished sample

3.2 Kolsky bar system

The mechanical properties of boron carbide was measured by Kolsky bar uniaxial compression test and X-ray phase contrast imaging (XPCI) performed at beamline 32-ID-C at APS. The image

was recorded by Shimadzu HPV-X2 camera. A schematic diagram is shown in the Fig.5.

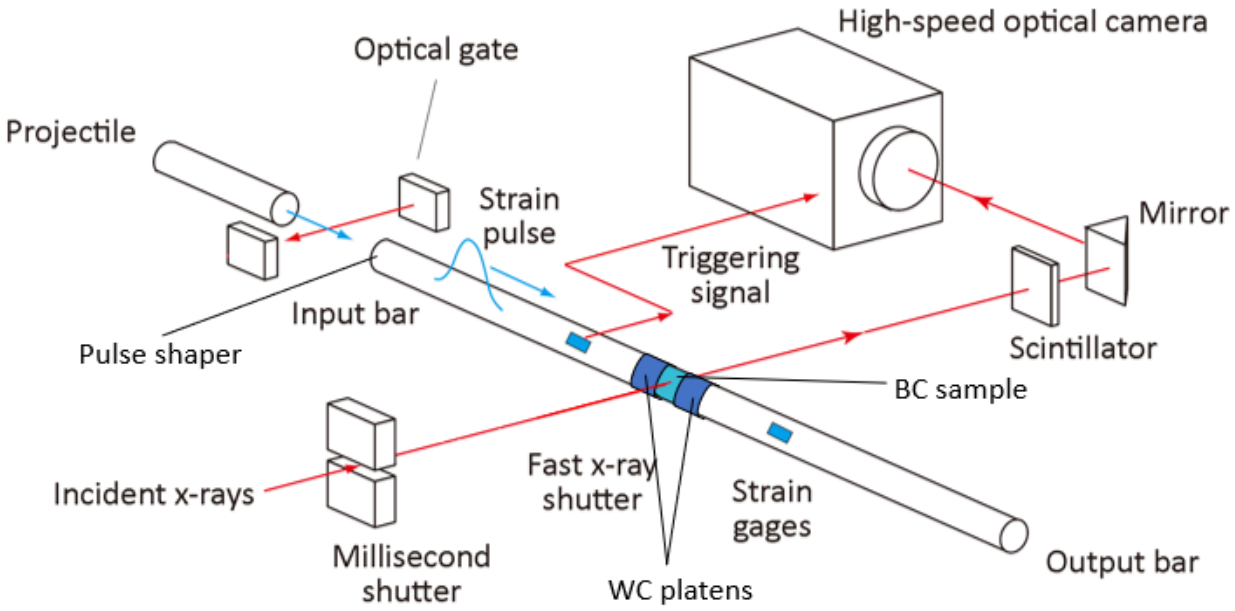

Fig.5. Schematic diagram of Kolsky bar along with high speed X-ray system

In the Kolsky bar system, the length of striker bar, input bar and output bar were 228.6mm (9”), 914.4mm (36”) and 508mm (20”) respectively. All of them were made in Maraging Steel C350 with 6.35mm (0.25”) in diameter. Between input bar and output bar, two 6.35mm (0.25”) in diameter tungsten carbide platens were placed to protect the bars by increasing impact contact area between bar and sample. Moreover, a 1mm long, 2.08mm diameter copper disk was placed between projectile and input bar, acting as pulse shaper, allowing both constant strain-rate deformation and dynamic stress equilibrium[9]. The stress and strain signal were measured by strain gages on incident bar and transmission bar. The gas gun was shot at pressure of 125 psi. We used Micro-Measurements® stain gages with a gage factor of 2.04 at room temperature,

which means 1V=2040μs, and grid resistance is 1000Ω. For input bar, strain rate is measure by half bridges, the input voltage is 2V, and grid resistance is 1000Ω. For output bar, strain rate is measure by half bridges, and the input voltage is 30V. The distance between sample to camera was 0.73m.

3.3 XPCI experiment

In the XPCI experiments, the energy of X-ray from synchrotron radiation was 20.4keV. The undulator gap is 12mm. The X-rays transmitted through the sample, converted into visible light by a 100 μm thick single-crystal $Lu_3Al_5O_{12}$:Ce scintillator, then refracted by mirror before captured by a 250×400 pixel Shimadzu HPV-X2 camera (Shimadzu Corporation).

The data analysis theory is the same with Leong's previous experiment[9]. 25 sets of experiments were performed in APS, with 15 sets recording complete results of XPCI images and mechanical properties. Results of four sets of experiments are shown in the next chapter and the rest of sets are in the appendix. For each experiment we recorded an image sequence of 128 frames. Two experiments were recorded under 5Mfps and the rest two were recorded under 1Mfps. The X-ray pulse was emitted every 153.4 ns, and the decay of intensity was submitted to exponential function.[10] So the camera recorded every either 200 ns or 1000 ns with only 110 ns actually acquiring image signal, which means each acquisition window will record light emitted from X-ray pulses in different intensity. Thus, the signal we received from the camera is shown in Fig.6. The intensity of each image is the area of each red line marked

region. Thus, in order to get rid of the influence of different recording windows to obtain normalized images, we need to divide the intensity index of each image by the area of X-ray pulses intensity of each frame.

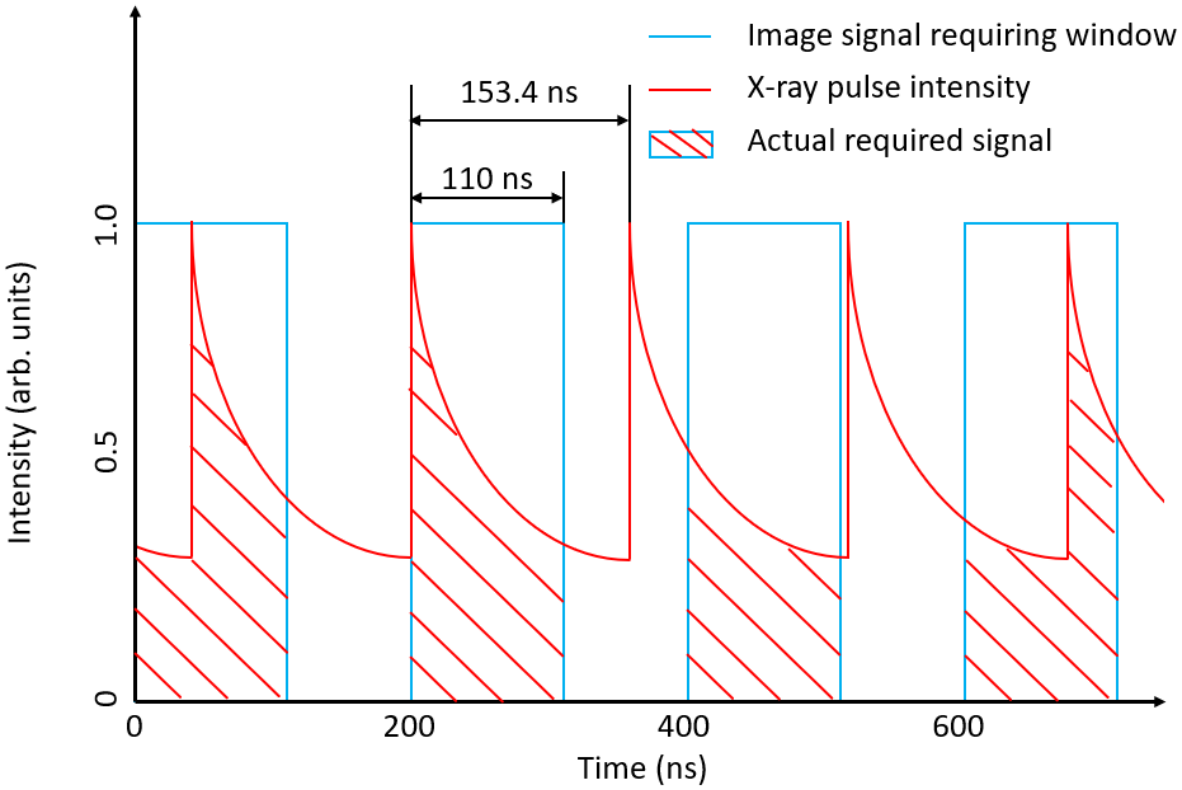

Fig.6. Working mechanism of scintillator and camera

4. Results

4.1 In situ visualization of fracture

The crack initiation and propagation of BC under dynamic loading was visualized by the high intensity X-ray's diffraction through the material, as shown in Fig.7.

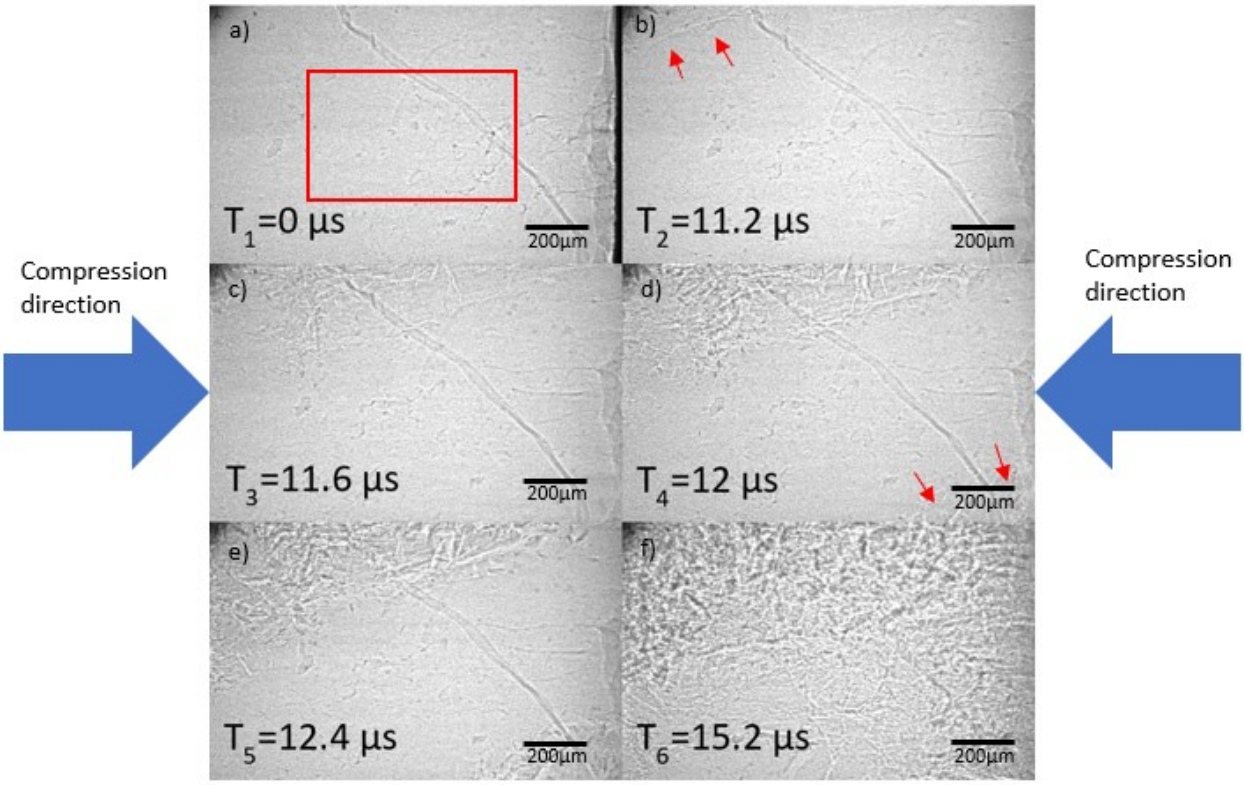

Fig.7. Crack initiation and propagation of BC under dynamic loading (sample BC65), a) starting time of camera recording, b) initiation of first crack on the edge, c) crack propagation, d) initiation of new cracks on another edge, e) crack propagation, f) sample failed

T=0 is defined as the starting time of camera recording. The first crack was observed at T=11.2 µs, when the stress was shortly past the stress peak. Cracks often initiated at the edge of the cuboid during dynamic loading, possibly due to stress concentration around the edge. After that, more cracks were generated, partly from adjacent region of the first crack, and partly from the other

edge of the sample. Finally the stress dropped quickly until the material failed.

4.2 Dynamic mechanical response

Our experiment shows that the peak stress of boron carbide under high strain loading is in the range of 2.5-4.0 GPa, which is in the range of with previous results [3,5-7,14]. The appendix includes the detail of each set of experiment and data.

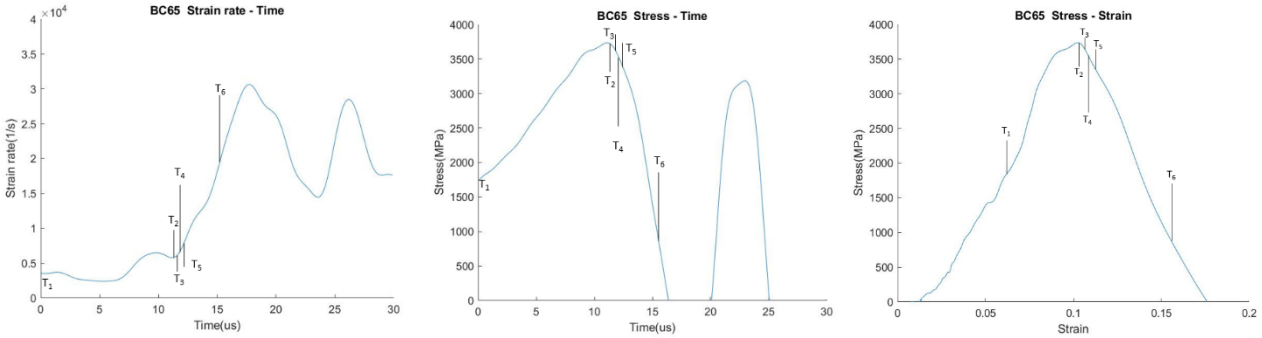

Fig.8. Dynamic mechanical response of BC (sample BC65)

Fig.8 shows the dynamic mechanical response of BC65, imaging at 5Mfps. At the time when the first crack is observed, stress reached the peak. Then with more crack generation, the stress decreased dramatically and the strain rate kept increasing until the sample failed. The same dynamic mechanical response as well as its relation with XPCI images under high strain rate was observed in all other sets of experiments, shown in Fig.9 and appendix. As a result, there are some correlations between XPCI images and dynamic mechanical properties, the combination of which is possible to be used to better understand the damage extent of boron carbide.

Fig.9 shows all other believable data of dynamic response of boron carbide. The reason that the data in the appendix is not completely believable is because the broken strain gages on the input bar during experiment make it hard to verify the accuracy of signal by comparing the signal of input bar with output bar.

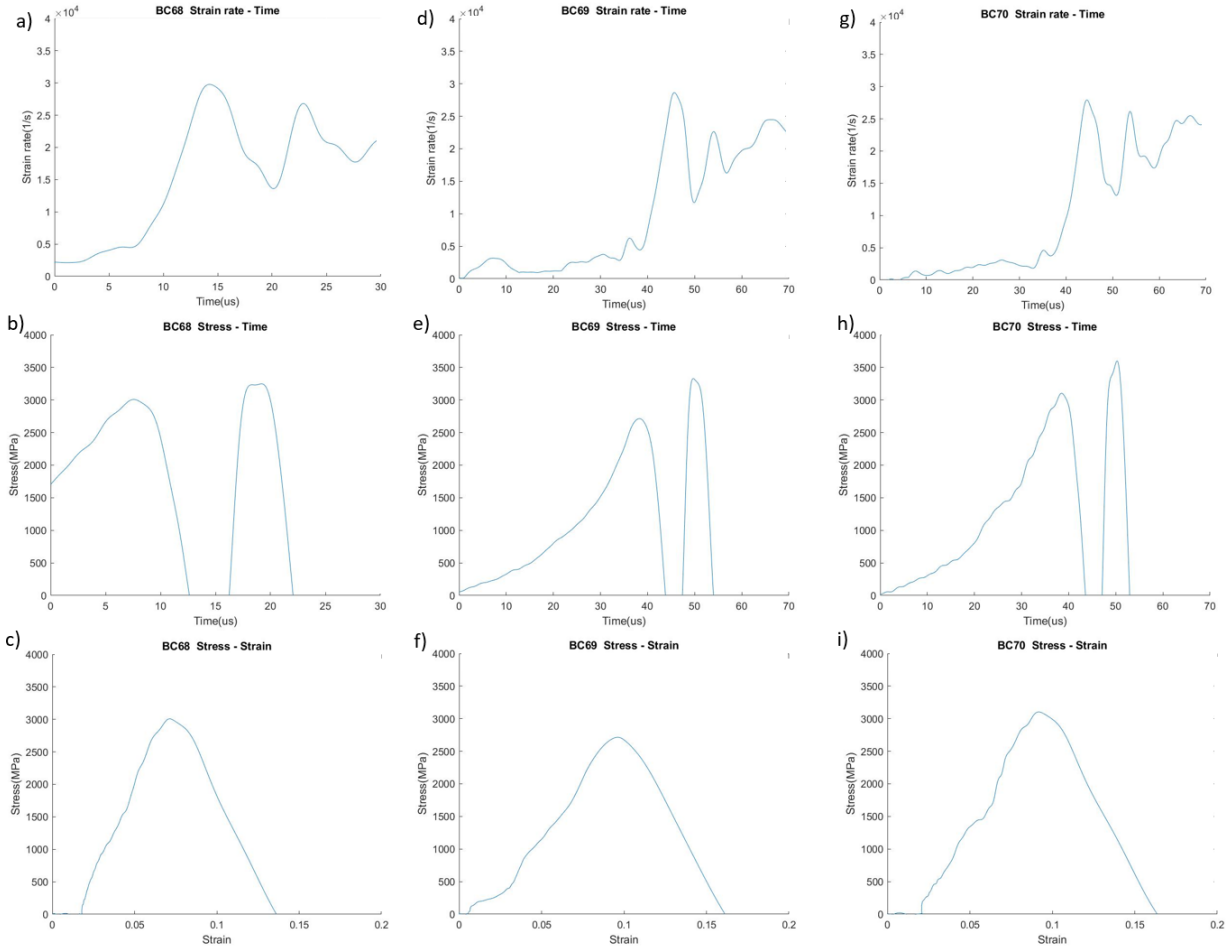

Fig.9. Dynamic mechanical response of BC (sample BC68, 69, 70)

4.3 Analysis of fracture images

In order to quantitatively analyze the damage of the samples, we first chose a 200×150 pixel

region at the center of image to rule out possible error from the edges, shown in Fig.7. a). Then the average intensity of ROI of each frame was calculated, as shown in Fig.10. b). We expected to see constant average intensity before crack initiation. However, around 10% fluctuation of intensity was observed before crack initiation. This can be explained by the inhomogeneous X-ray pulse intensity from the beamline, which has 10% energy fluctuation.

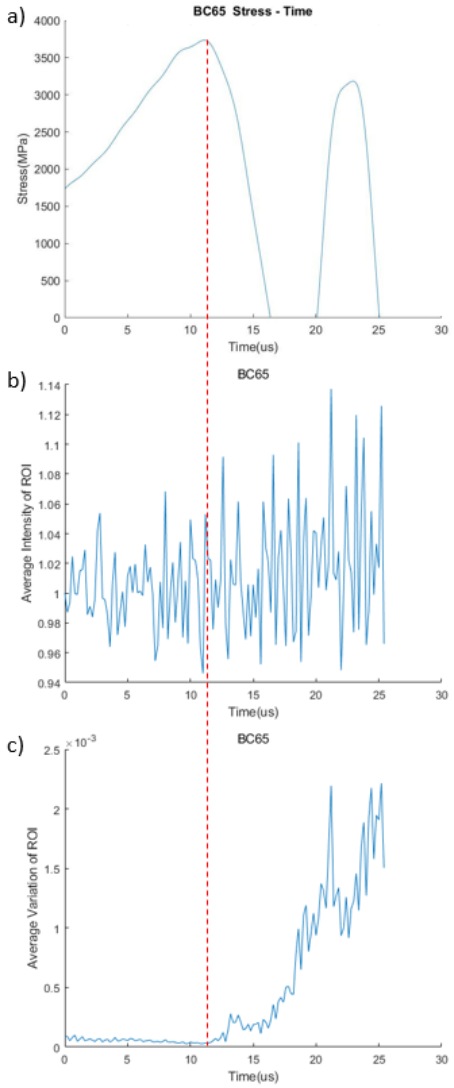

Fig.10. Analysis of fracture images of ROI of BC (sample BC65), a) stress-strain curve, b) average intensity of ROI, c) average variation of ROI

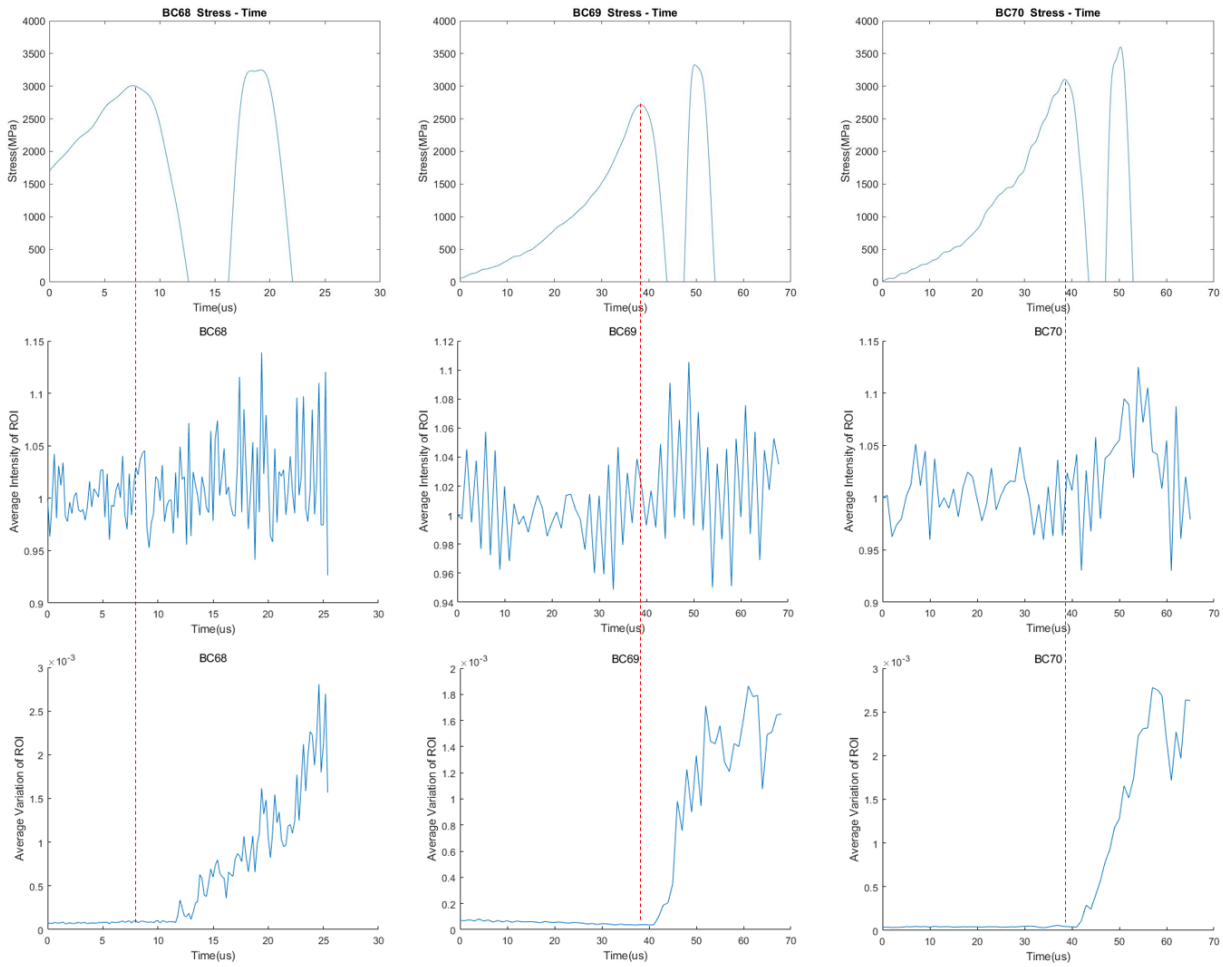

Fig.11. Analysis of fracture images of ROI of BC (sample BC68, 69, 70)

To rule out the error of X-ray source, the average variation of ROI was calculated in Fig.10. c). The variation was almost constant before crack initiation. Then the variation increased dramatically with crack propagation and crack generation. Moreover, we observed some delay of the increase of variation compared with the peak stress. This can be explained by the generation of cracks at the edge of sample where the ROI didn't include it. Since the crack number, size and distribution cause the phase shift and thus causing variation, the variance of the image intensity in a region of interest can be used as a semi-quantitative measure of degree of damage, and that trends in

damage derived from this measure correlate with the stress-strain behavior of the material.

The analysis data of BC68, 69, 70 are shown on Fig.11. to show the consistence of the result.

4.4 Physics model for XPCI

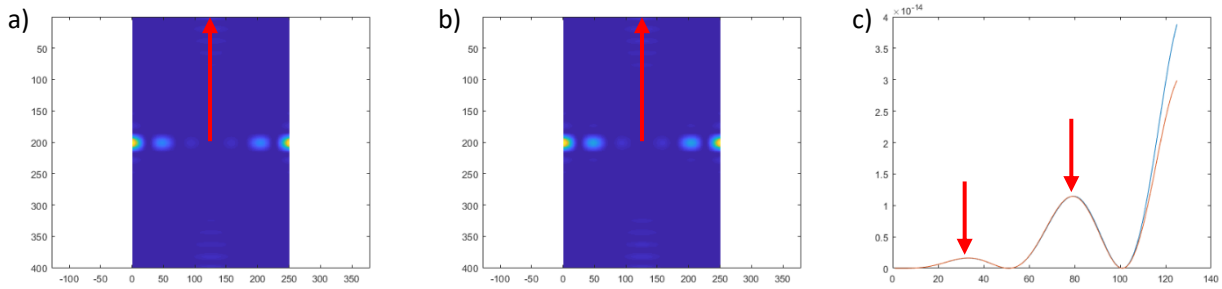

Fig.12. Power spectrum of XPCI simulation with a single crack at L=0.001m, a) power spectrum of simulating result (left side of equation), b) power spectrum of analytical result (right side of equation), c) power spectrum intensity along vertical direction for both

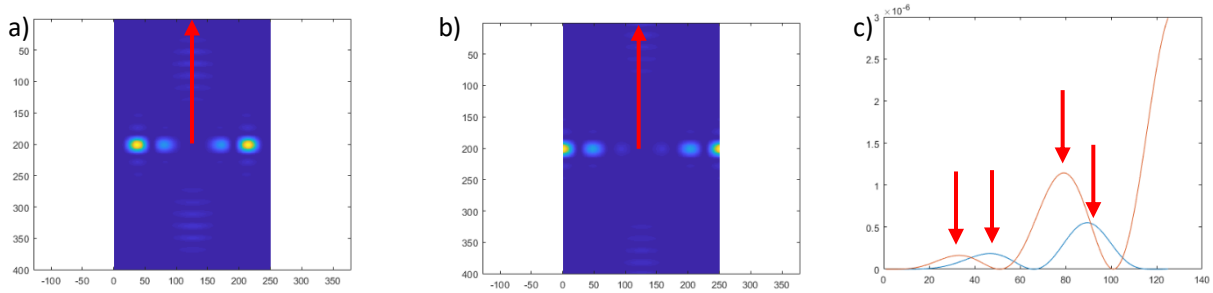

Fig.13. Power spectrum of XPCI simulation with a single crack at L=0.73 m, a) power spectrum of simulating result (left side of equation), b) power spectrum of analytical result (right side of equation), c) power spectrum intensity along vertical direction for both

We tried to use a model developed by Leong[15] mentioned before to obtain crack number and distribution during loading.

$$\left|F\left\{\frac{I(x,y,z=L)}{I(x,y,z=0)}-1\right\}\right|^2=\sum(L^2\delta^2{k_\perp}^4|8abc\mathrm{sinc}(a)\mathrm{sinc}(b)\mathrm{sinc}(c)|^2), \qquad (1)$$

This model described a method to extract crack information inside a sample from near-field XPCI

images. To testify the feasibility of the model on our experiment, we modeled a single crack at the size of 40×4×4 pixel, as shown in Fig.12 and Fig.13.

The result of model is shown in Fig.12, when the assuming distance between sample and camera is very small (L=0.001m), the simulating result and analytical result match well. We testified that we can model a single crack at L=0.0001m, when near-field diffraction happens. In this case, we could model multiple cracks in any number, size and distribution and check the correctness of the model by checking if the first several peaks of the simulating result and analytical result match well.

However, for our experiment at L=0.73m, the peaks of power spectrum shift and don't match any more (Fig.13). This is because the model is only suitable for near-field, while our experiment is a far-field diffraction (the Fresnel number of which is 0.2). Thus, some modification for far-field diffraction is needed to make the model suitable to characterize the damage extent and evolution under our experimental condition. This model is also potentially useful for calibrating and validating brittle fracture models currently being developed for a wide variety of materials.

5. Discussion

We demonstrate that it is feasible to prepare small boron carbide cuboid samples in dimension of 1.5 mm and finish with 1 μs polishing paper. We combined kolsky bar uniaxial compression bar system with phase contrast imaging technique to visualize the failure in real time, which is correlated with dynamic mechanical properties. And the combination of them is possible to be used to better understand the damage extent of boron carbide.

We observed the stress of boron carbide under high strain rate in the range of 2.7-3.8 GPa, and strain rate at failure in the range of 6,000-11,000. The cracks always initiate at the edge of the sample because of stress concentration at that area.

We visualized the failure in real time using x-ray phase contrast imaging (XPCI) at the Advanced Photon Source. We can clearly see the crack initiation and propagation during the process but due to the inhomogeneous x-ray source pulse, we cannot process the images to the same level of intensity. Instead, we utilized the variance of the images to rule out the error of X-ray source and hoped to be used as a semi-quantitative measure of degree of damage with mechanical properties we obtained. All other experimental results are enclosed in appendix.

Finally, we tried to utilize physics model proposed by Leong to model the crack number, distribution and orientation of the specimen. However, some modification for far-field diffraction is needed to make the model suitable to characterize the damage extent and evolution under our

experimental condition.

Appendix

The parameter of each set of experiment is shown below.

Sample	Length (mm)	Width (mm)	Height (mm)	Pressure (PSI)	Notes
BC65	1.363	1.385	1.34	125	image at 5Mfps.
BC69	1.364	1.38	1.345	125	image at 1Mfps.
BC70	1.369	1.378	1.351	125	image at 1Mfps.
BC68	1.36	1.378	1.355	125	image at 5Mfps.
BC47	1.618	1.76	1.346	125	image at 1Mfps.
BC71	1.323	1.379	1.351	125	image at 5Mfps.
BC67	1.37	1.374	1.358	125	image at 5Mfps.
BC63	1.367	1.378	1.345	125	image at 5Mfps.
BC53	1.654	2.807	1.5	175	image at 1Mfps
BC54	1.648	2.809	1.474	175	image at 1Mfps
BC57	1.643	2.804	1.49	175	Image at 5Mfps
BC58	1.64	2.807	1.488	175	Image at 5Mfps
BC59	1.644	2.814	1.496	175	Image at 5Mfps
BC60	1.653	2.811	1.499	175	Image at 5Mfps

Table.2 Parameters of each set of experiment

The mechanical properties results, as well as the intensity and variance of images are shown below. The data in the appendix is not completely believable because the broken strain gages on the input bar during experiment make it hard to verify the accuracy of signal by comparing the signal of input bar with output bar.

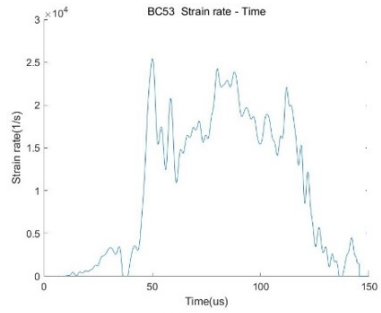
BC53 Strain rate - Time
Strain rate(1/s)
Time(us)

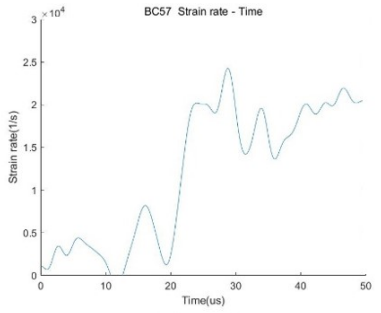
BC57 Strain rate - Time
Strain rate(1/s)
Time(us)

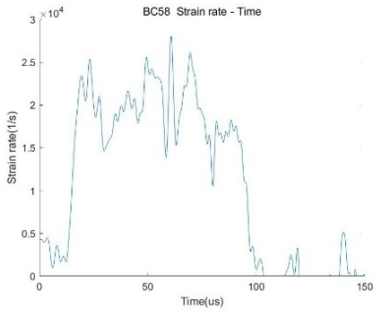
BC58 Strain rate - Time
Strain rate(1/s)
Time(us)

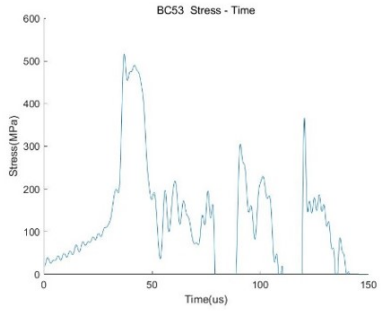
BC53 Stress - Time
Stress(MPa)
Time(us)

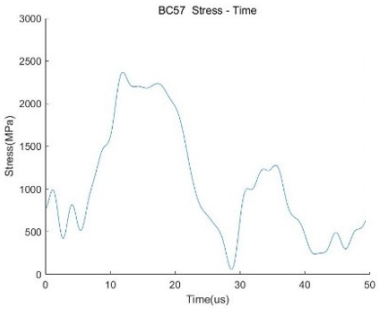
BC57 Stress - Time
Stress(MPa)
Time(us)

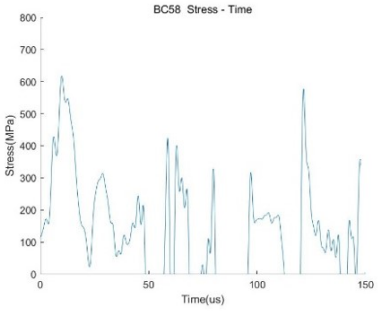
BC58 Stress - Time
Stress(MPa)
Time(us)

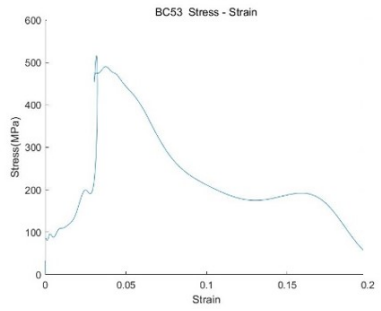
BC53 Stress - Strain
Stress(MPa)
Strain

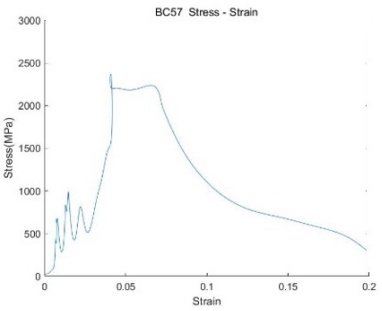
BC57 Stress - Strain
Stress(MPa)
Strain

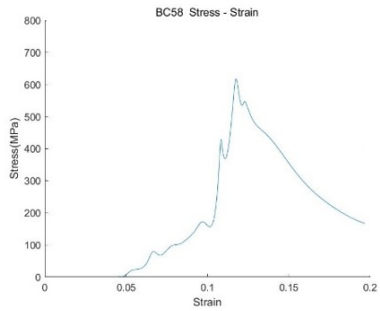
BC58 Stress - Strain
Stress(MPa)
Strain

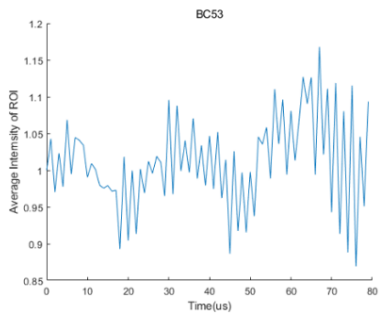
BC53
Average Intensity of ROI
Time(us)

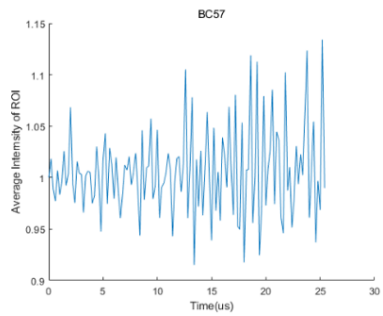
BC57
Average Intensity of ROI
Time(us)

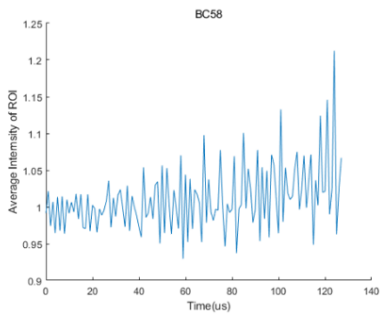
BC58
Average Intensity of ROI
Time(us)

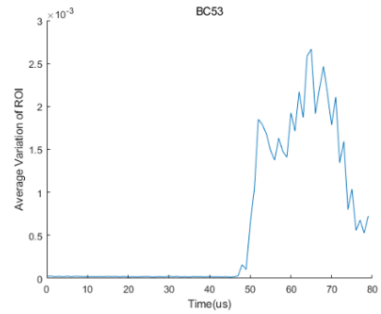
BC53
Average Variation of ROI
Time(us)

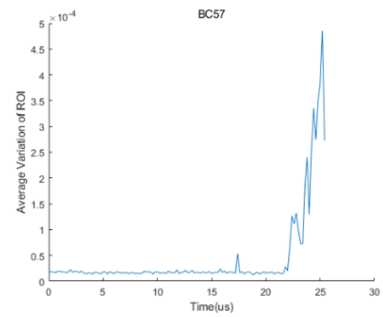
BC57
Average Variation of ROI
Time(us)

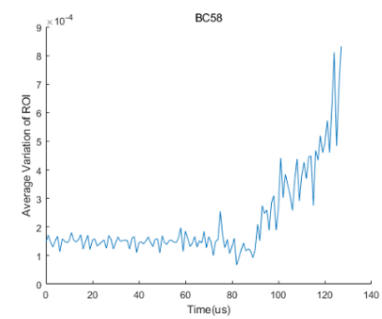
BC58
Average Variation of ROI
Time(us)

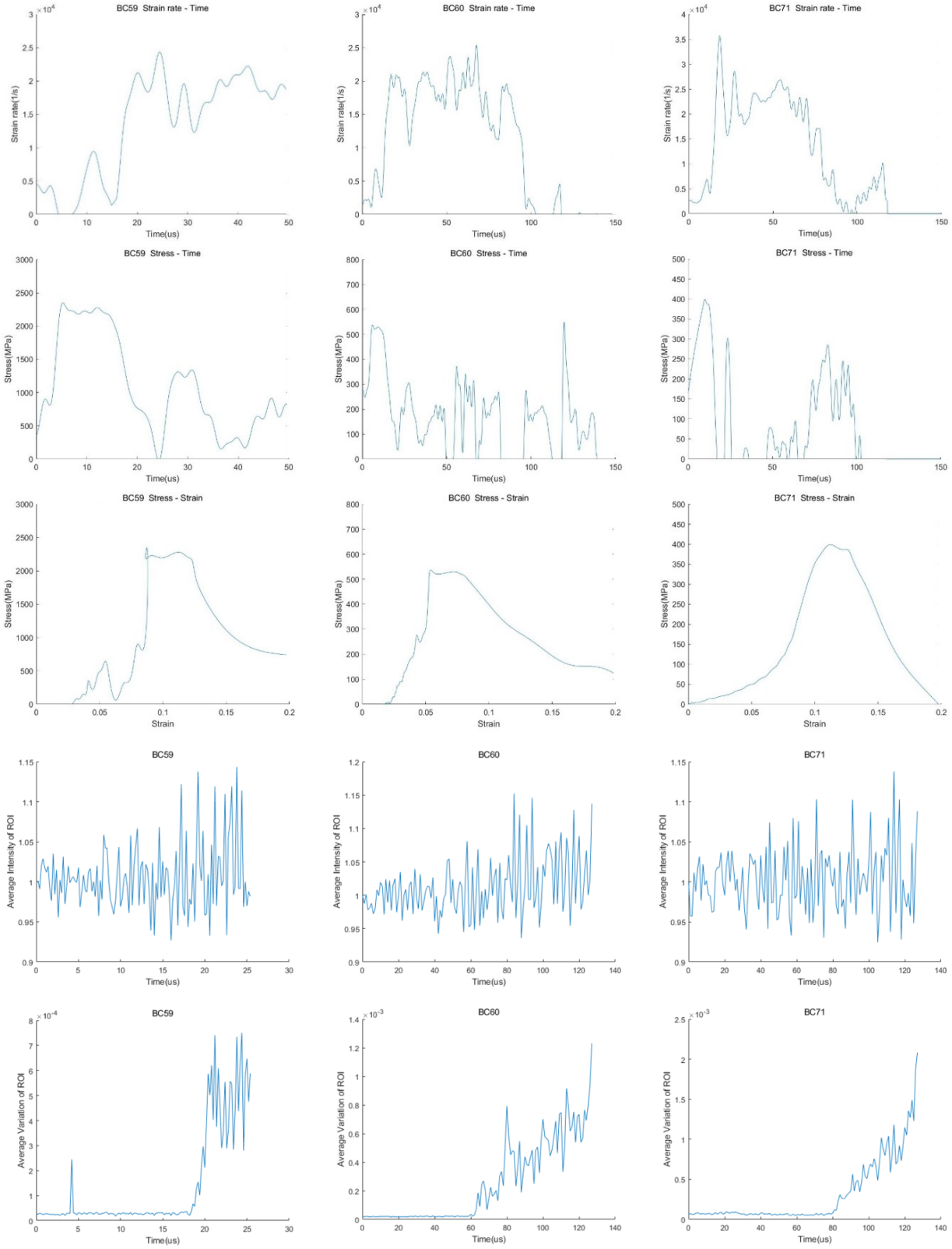
BC59 Strain rate - Time
Strain rate(1/s)
Time(us)
BC60 Strain rate - Time
Strain rate(1/s)
Time(us)
BC71 Strain rate - Time
Strain rate(1/s)
Time(us)
BC59 Stress - Time
Stress(MPa)
Time(us)
BC60 Stress - Time
Stress(MPa)
Time(us)
BC71 Stress - Time
Stress(MPa)
Time(us)
BC59 Stress - Strain
Stress(MPa)
Strain
BC60 Stress - Strain
Stress(MPa)
Strain
BC71 Stress - Strain
Stress(MPa)
Strain
BC59
Average Intensity of ROI
Time(us)
BC60
Average Intensity of ROI
Time(us)
BC71
Average Intensity of ROI
Time(us)
BC59
Average Variation of ROI
Time(us)
BC60
Average Variation of ROI
Time(us)
BC71
Average Variation of ROI
Time(us)

Reference

[1] Paliwal, B., and K. T. Ramesh. "Effect of crack growth dynamics on the rate-sensitive behavior of hot-pressed boron carbide." Scripta materialia 57.6 (2007): 481-484.

[2] Xie, Kelvin Y., et al. "Microstructural characterization of boron-rich boron carbide." Acta Materialia 136 (2017): 202-214.

[3] Domnich, Vladislav, et al. "Boron carbide: structure, properties, and stability under stress." Journal of the American Ceramic Society 94.11 (2011): 3605-3628.

[4] Chen, Mingwei, James W. McCauley, and Kevin J. Hemker. "Shock-induced localized amorphization in boron carbide." Science 299.5612 (2003): 1563-1566.

[5] Savinykh, A. S., et al. "Dynamic strength of reaction-sintered boron carbide ceramic." Technical Physics 60.6 (2015): 863-868.

[6] Swab, Jeffrey J., et al. "Static and dynamic compression strength of hot-pressed boron carbide using a dumbbell-shaped specimen." Journal of Materials Science 52.17 (2017): 10073-10084.

[7] Hayun, S., et al. "Static and dynamic mechanical properties of boron carbide processed by spark plasma sintering." Journal of the European Ceramic Society 29.16 (2009): 3395-3400.

[8] Leong, Andrew FT, et al. "Quantitative in situ studies of dynamic fracture in brittle solids using dynamic X-ray phase contrast imaging." Experimental Mechanics 58.9 (2018): 1423-1437.

[9] Heard, W. F., et al. "Annular pulse shaping technique for large-diameter Kolsky bar

experiments on concrete." Experimental Mechanics 54.8 (2014): 1343-1354.

[10] Luo, S. N., et al. "Gas gun shock experiments with single-pulse x-ray phase contrast imaging and diffraction at the Advanced Photon Source." Review of Scientific Instruments 83.7 (2012): 073903.

[11] Feng, Z. D., et al. "Dynamic damage and fracture of a conductive glass under high-rate compression: A synchrotron based study." Journal of Non-Crystalline Solids 494 (2018): 40-49.

[12] Huang, J. Y., et al. "Dynamic deformation and fracture of single crystal silicon: Fracture modes, damage laws, and anisotropy." Acta Materialia 114 (2016): 136-145.

[13] Ghosh, Dipankar, et al. "Influence of stress state and strain rate on structural amorphization in boron carbide." Journal of applied physics 111.6 (2012): 063523.

[14] Paliwal, B., and K. T. Ramesh. "Effect of crack growth dynamics on the rate-sensitive behavior of hot-pressed boron carbide." Scripta materialia 57.6 (2007): 481-484.

[15] Leong, Andrew FT, et al. "Measurement of absolute regional lung air volumes from near-field x-ray speckles." Optics express 21.23 (2013): 27905-27923.

[16] Chen, Weinong W., and Bo Song. Split Hopkinson (Kolsky) bar: design, testing and applications. Springer Science & Business Media, 2010.

[17] D. Paganin, S. C. Mayo, T. E. Gureyev, P. R. Miller, and S. W. Wilkins, “Simultaneous phase and amplitude extraction from a single defocused image of a homogeneous object,” J. Microscopy 206, 33–40 (2002).

[18] Buyuka, B., et al. "Investigation on the Effects of Boron Carbide Particle Size on

Radiation Shielding Properties of Boron Carbide Titanium Diboride Composites." (2013).

[19] Cheng, Chun, et al. "Structure and mechanical properties of boron-rich boron carbides." Journal of the European Ceramic Society 37.15 (2017): 4514-4523.

[20] Ling, Wang, et al. "Structure and Mechanical Properties of Densified Boron Carbide Ceramics by SPS." Rare Metal Materials and Engineering 38 (2009): 529-532.

[21] Han, Zenghu, et al. "Microstructure and mechanical properties of boron carbide thin films." Materials Letters 57.4 (2002): 899-903.

[22] Khan, Atta U., Vladislav Domnich, and Richard A. Haber. "Boron carbide-based armors: problems and possible solutions." American Ceramic Society Bulletin 96.6 (2017): 30-35.

[23] Domnich, Vladislav, et al. "Boron carbide: structure, properties, and stability under stress." Journal of the American Ceramic Society 94.11 (2011): 3605-3628.

[24] An, Qi, William A. Goddard III, and Tao Cheng. "Atomistic explanation of shear-induced amorphous band formation in boron carbide." Physical review letters 113.9 (2014): 095501.

[25] Lazzari, R., et al. "Atomic structure and vibrational properties of icosahedral B4C boron carbide." Physical review letters 83.16 (1999): 3230.

[26] Roberson, C. J., et al. "The effective hardness of hot pressed boron carbide with increasing shock stress." Advances in Ceramic Armor: A Collection of Papers Presented at the 29th International Conference on Advanced Ceramics and Composites, January 23-28, 2005, Cocoa Beach, Florida, Ceramic Engineering and Science Proceedings. Vol.

26. Hoboken, NJ, USA: John Wiley & Sons, Inc., 2005.

[27] Olbinado, Margie P., et al. "MHz frame rate hard X-ray phase-contrast imaging using synchrotron radiation." Optics express 25.12 (2017): 13857-13871.

Biography

Jiajie Huang was born in 1995 in China.

Jiajie Huang did his undergraduate work in Tongji University in China where he majored in Materials Science and Engineering. During his undergraduate studies, he focused on building materials and finish his thesis “Study on Strengthening and Toughening of Solid Waste Based Geopolymer”. Jiajie also spent a semester to study in The Technical University of Madrid in civil engineering department, working on calculating softening curve of SFRC under impact.

In 2017, Jiajie joined Todd C. Hufnagel’s group in Johns Hopkins University as a master’s student to study dynamic properties of boron carbide and the method to model damage extent.